J. Fluid Mech. (2003), *vol.* 491, *pp.* 183–205.
DOI: 10.1017/S0022112003005482 Printed in the United Kingdom

The influence of the thermal diffusivity of the lower boundary on eddy motion in convection

By J. C. R. HUNT[1,2], A. J. VRIELING[2], F. T. M. NIEUWSTADT[2] AND H. J. S. FERNANDO[3]

[1]Department of Space and Climate Physics, University College London, Gower Street, London WC1E 6BT, UK

[2]J. M. Burgers Centre for Fluid Dynamics, Delft University of Technology, Leeghwaterstraat 21, 2628 CA Delft, The Netherlands

[3]Environmental Fluid Dynamics Program, Arizona State University, Tempe, AZ 85287, USA

(Received 12 June 2002 and in revised form 21 January 2003)

The paper presents new concepts and results for the eddy structure of turbulent convection in a horizontal fluid layer of depth h which lies above a solid base with thickness h_b. The fluid parameters are the kinematic viscosity ν, the thermal diffusivity κ, which is taken to be comparable with ν, the density ρ, the specific heat c_p and the expansion parameter β. The thermal diffusivity of the solid is κ_b. The results are an extension of the more commonly studied cases, where a constant heat flux or constant temperature is applied at the interface between the fluid and the base. The buoyancy forces induce eddy motions with a typical velocity $w_* \sim (g\beta F_\theta h)^{1/3}$ where $\rho c_p F_\theta$ is the average heat flux and F_θ the covariance of the fluctuations of the temperature and of the vertical velocity. At moderate Reynolds numbers ($Re = w_* h/\nu$), say less than about 10^3, an order-of-magnitude analysis shows that for the case of high diffusivity of the base (i.e. $\kappa_b \gg \kappa$) elongated 'plumes' form at the surface and extend to the top of the fluid layer. When the base diffusivity is low (i.e. $\kappa_b \leqslant \kappa$) the surface cools below the developing 'plume' and either the plume breaks up into elongated puffs or, if $\kappa_b \ll \kappa$, horizontal pressure gradients form so that only small-scale puffs can form near the surface. At very high Reynolds numbers, approximately greater than 10^4, the surface boundary layer below each puff/plume is highly turbulent with a local logarithmic velocity and temperature profile. An approximate analysis indicates for this case that there is insufficient buoyancy flux from the base, irrespective of its diffusivity, to maintain plumes, because of the high turbulent heat transfer. So puffs dominate high-Reynolds-number thermal convection as numerical simulations and field experiments demonstrate. However, when the surface heat flux is uniform, for example as a result of radiant heat transfer or by forcing with a constant heat flux below a very thin conducting base, plumes are the dominant form of eddy motion, as is commonly observed. In the numerical solutions presented here, where $Re \sim 3 \times 10^2$ and the slab thickness $h_b = h$, it is shown that the spatial scales of eddy structures in the fluid layer close to the surface become significantly smaller as κ_b/κ is reduced from 100 to 0.1. At the same time in the core of the convective layer the change in the autocorrelation and spatial correlation function indicates that there is a transition from long-duration plumes into shorter-duration and smaller-length-scale elongated puffs. The simulations show that the largest temperature fluctuations near the surface occur when a constant heat flux is applied at the bottom of the fluid layer. The smallest temperature fluctuations are associated with the constant-temperature boundary condition. The finite base diffusivity cases lie in between these limits, with the largest fluctuations occurring when the thermal diffusivity of the base is

small. The hypothesis introduced above has been tested qualitatively in a laboratory set-up when the effective diffusivity of the base was varied. The flow structure was observed as it changed from being characterized by nearly steady plumes, into unsteady plumes and finally into puffs when the thickness of the conducting base was first increased and then the diffusivity was decreased.

1. Introduction

Our modern understanding of turbulent flows is based on a dual description and analysis in terms of the statistics of the velocity, pressure and other variables and in terms of the structure and time dependence of the details of the eddy motion (e.g. Holmes, Lumley & Berkooz 1996). The latter aspects of these random multi-scale flows is particularly useful for developing quasi-deterministic models for the dynamics and thermodynamic properties of the flow (e.g. the magnitude of the velocity fluctuations in terms of the macroscopic features of the flow) and for other processes that depend on these properties (e.g. the movement of solid particles or chemical reactions).

The flow that we consider consists of a fluid layer with depth h above a solid layer with depth h_b (see figure 1). At the bottom of the base ($x_3 = -h_b$) a uniform and constant heat flux H_0 is applied which is transmitted by conduction through the solid base and which drives the convection in the fluid layer. At $x_3 = h$ there is an insulating solid surface where the heat flux is zero. Thus the mean temperature steadily rises. The mean heat flux at the bottom of the fluid layer is given by $H = \rho_0 c_p F_\theta$ where ρ_0 is the reference fluid density, c_p the specific heat at constant pressure and $F_\theta \equiv \overline{w'\theta'}$ is the correlation between the vertical velocity and temperature fluctuations.

The study of convective turbulence is a conspicuous example of where the 'eddy-structure' approach is valuable. In this flow regime the effects of buoyancy forces are much greater than those produced by shear stresses τ ($=\rho_0 u_*^2$, where u_* is the friction velocity) associated with any mean motion. As a result the shear-buoyancy Monin–Obukhov length $L_{MO} = u_*^3/(g\beta F_\theta)$ is much smaller than the depth of the layer. Here β is the coefficient of expansion with $\beta \simeq 1/T_0$ for a perfect gas (e.g. Holtslag & Nieuwstadt 1986). The aim of this paper is to study in more detail the current 'conventional wisdom' about the eddy structure.

Recent reviews and theories (e.g. Hunt, Kaimal & Gaynor 1988; Castaing 1989 *et al.*; Lohse & Grossmann 2000) have described many features of turbulent thermal convection on the assumption that the eddy structure can be approximated by thin energetic vertical plumes (see figure 2) of hot fluid extending from the bottom plate right to the top, with weak cooler flow between the plumes descending down into thin energetic 'feeder' layers with depth ℓ (see figure 1) at the lower plate where the fluid is heated before entering the plumes. This concept was originally established by Priestley (1959) on the basis of his multi-point measurements in the atmospheric boundary layer over the hot Australian desert. He pointed out that Morton, Taylor & Turners's (1956) analysis of turbulent plumes indicated the essential scaling for the distributed plumes in convection, and that the root-mean-square velocity $\sigma_w \sim w_* \sim (g\beta F_\theta h)^{1/3}$, a result later revisited by Deardorff, Willis & Lilly (1967) and confirmed in the atmosphere by Kaimal *et al.* (1976). Note that $h/L_{MO} = (w_*/u_*)^3 \gg 1$ for these flows.

However, as Scorer (1954, 1978) pointed out, in the atmospheric boundary layer there are many occasions when the eddy structure is in the form of isolated 'puffs' (see figure 2), i.e. local regions of correlated motion with diameter significantly less than

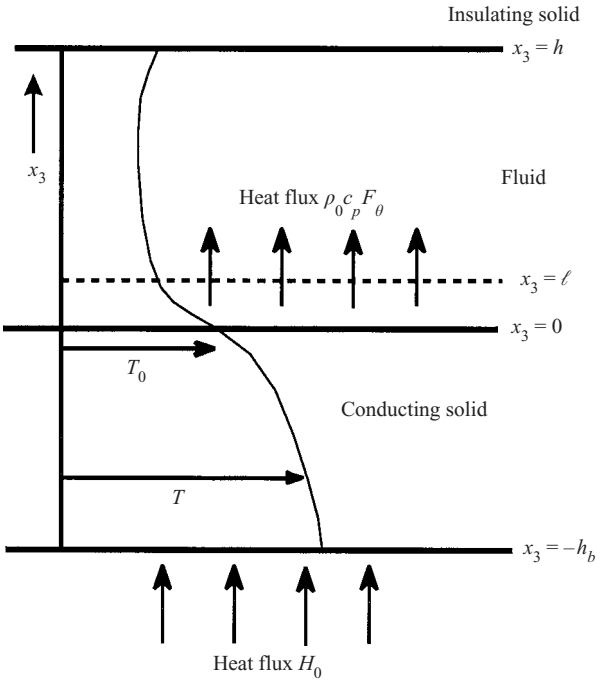

FIGURE 1. Schematic representation of the mean temperature profile in a convective fluid layer ($h < z < 0$) and in a solid base ($0 < z < h_b$) with a uniform heat flux H_0 at the bottom of the base.

h where the fluid is more buoyant than in the surroundings (and above and below it) so that these puffs rise with respect to the surrounding fluid. These structures have been noted by glider pilots and observers of soaring birds in conditions of weak convection, e.g. the U.K. and even in desert conditions in the U.S.A (in the evening).

The heat transfer results, velocity statistics and visualization studies obtained in laboratory experiments on convection (notably those of Deardorff *et al.* 1967) are consistent with the quantitative predictions resulting from Priestley's plume model. However, other results on the eddy structure have been reported. For instance, Townsend's (1959) clear experimental observation of puffs has been regarded hitherto as a 'curiosity'. Progressively, since the 1960s direct and large-eddy numerical simulations have been used to study turbulent convection. In all the simulations reported up to now the bottom boundary condition has been that of a constant heat flux. In these studies it has always been found that the eddy structure consists of plumes.

Despite this consensus among professional fluid dynamicists over the past 40 years, practioners in the kitchen (and elsewhere) have known (e.g. M. E. Hunt, private communication) that the transition in the eddy structure between plumes and puffs is no mystery and can indeed be controlled. The purpose is to make the eddy movement rapid and well distributed enough that no point on the surface becomes too hot (to overheat milk) or that solid particles (in jam making) come to rest on the bottom. This is done by varying the thermal conductance of the solid base through which the fluid layer is heated. Introduction of low-conductance simmering plates or asbestos sheets (as in Townsend's 1959 experiments) transforms the plume-like eddies into

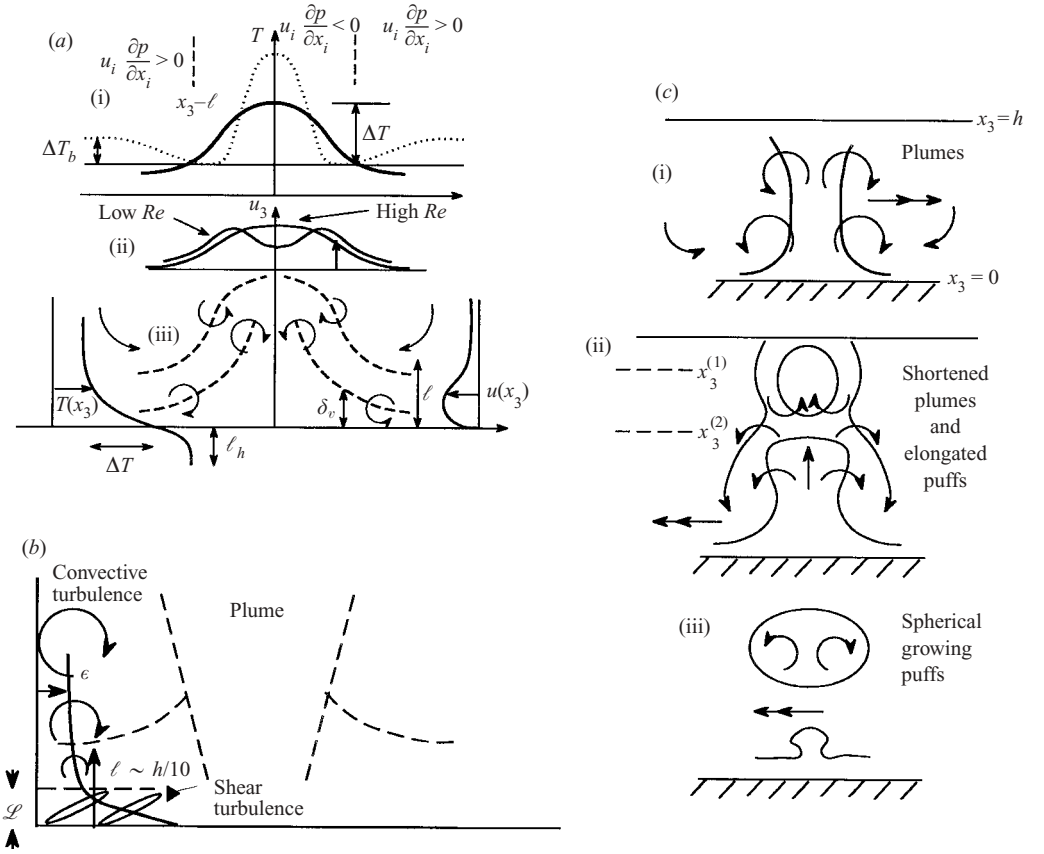

FIGURE 2. Schematic diagram of typical profiles of key variables and mechanisms in the zone near the surface where plumes originate. (*a*) (i) Temperature $T(x)$ just above the surface layer and at the surface; (ii) vertical velocity (in high- and low-Reynolds-number flows); (iii) instantaneous vertical profiles of the temperature $T(x_3)$, the horizontal velocity $u_1(x_3)$ and the vorticity distributions corresponding to the surface layer and the surface viscous layer. (*b*) At very high Reynolds number ($\ll 10^4$) there is a surface layer of thickness $\mathscr{L}$ where the energy dissipation ϵ is much greater than in the convective layer above and where the eddy structure is shear dominated instead of convectively driven. (*c*) The three types of buoyant eddy structure depending on the ratio of the base to layer diffusivity κ_b/κ and the Reynolds number: (i) plume; (ii) shortened plume or elongated puff; (iii) puff. The double arrow indicates how such eddies move horizontally in random directions as a result of the velocity fields of other eddies; this gives rise to regions of warmer fluid near the lower surface on the trailing side of these eddies (see § 4). The dashed horizontal lines in (ii) indicate levels where the buoyancy flux is greater at $x_3^{(1)}$ than at $x_3^{(2)}$ (as a result of a lower base diffusivity) which causes the plume to break up.

puff-like eddies. A similar unsteady puff convection phenomenon has been observed in some numerical simulations of very high-Reynolds-number geophysical convection patterns such as in the Earth's liquid core which are driven by the heat flux from the inner core (Höllerbach & Jones 1993). Another example is the 'compositional' convection in the polar oceans driven by the downward buoyancy flux of salty liquid generated near the sea surface by the freezing of ice as shown by the computation of Backhaus & Kämpf (1999) and the recent field observations by Uscinski *et al.* (2003).

A simple physical argument, which is quantified in § 2, explains the transition from plumes to puffs. If the conductance of a thick solid base is too low, the heat flux into the top layer of the solid is too small to balance the heat taken away by the growing plume or puff in the fluid surface (or feeder) layer. The local cooling at the surface causes horizontal pressure gradients that effectively 'shut off' the plume or puff which has to re-form at another point on the surface. Even if plumes are well established, this process may break them up because they are quite sensitive to any reduction in the heat/buoyancy being fed into them from the slightly cooled layer below. As we shall see this argument raises the question of why long-lasting plumes form at all in natural flows. A possible answer is given in § 6.

The physical arguments for convection in the form of plumes and puffs, as proposed by Hunt (1998) are tested here with some detailed analysis and with a numerical simulation and an experimental study of thermal convection over solid layers of varying diffusivity.

2. Order-of-magnitude physical analysis

We consider a thermally conducting slab or solid base lying between the levels $x_3 = -h_b$ and $x_3 = 0$ with thermal diffusivity κ_b. Above this base, between $x_3 = 0$ and $x_3 = h$ there is a layer of fluid with thermal diffusivity κ and kinematic viscosity ν (see figure 1). Above $x_3 = h$ there is an insulating solid (or approximately stationary fluid above a stable inversion layer). A uniform vertical heat flux H_0 is applied below the solid base. At the bottom of the fluid layer, i.e. $x_3 = 0$, this flux is reduced to $\rho c_p F_\theta = H_0 h/(h + h_b)$. The mean temperature at the interface at $x_3 = 0$ is T_0, and at $x_3 = h$ is T_h.

Several studies of convective turbulence (e.g. Lohse & Grossmann 2000) have derived order-of-magnitude expressions for the heat transfer (or Nusselt number, Nu) as functions of temperature difference (or Rayleigh number, Ra). As in those studies, we first assume that the flow near the surface, i.e. in the surface layer, is not fully turbulent, even though the turbulence in the interior is fully developed with chaotic motions over a wide range of space and time scales. Our focus is on how eddy motion depends on boundary conditions and on the Reynolds and Péclet numbers of the flow, where

$$Re = \frac{w_* h}{\nu}, \quad Pe = \frac{w_* h}{\kappa}. \tag{2.1}$$

The convective velocity scale w_* is defined by

$$w_* = (g\beta F_\theta h)^{1/3}, \tag{2.2}$$

where F_θ is defined in terms of the heat flux H (see § 1). Equation (2.2) gives the order of magnitude of the r.m.s. velocity in the interior of the flow, as will become apparent from the numerical results to be presented below.

When the Reynolds and Péclet numbers lie in the range $1 \ll Re \leqslant 10^2$ and $1 \ll Pe \leqslant 10^2$, the eddies develop as Rayleigh–Taylor bulge-like instabilities growing on the heated surface layer. Their horizontal scale is of the order of the thickness ℓ of this layer. Across these bulges the temperature drop is ΔT (see figure 2 and Lohse & Grossmann 2000). The vorticity generated on the edge of the bulge, which is in proportion to $-(\nabla\rho \times \nabla p)/\rho^2$, amplifies the vertical velocity w_l and converts the bulge into an upward moving 'puff'. Balancing inertial and buoyancy terms shows

that

$$w_l \sim (g\beta \Delta T\, \ell)^{1/2} \sim w_*. \tag{2.3}$$

The assumption here that $w_l \sim w_*$, which will verified later, is based on the fact that the velocity in the plume or puff is most intense at the top of the surface layer† where the plumes/puffs originate and decreases as they rise and grow. Note that there is a horizontal velocity into the growing puff/plume and because this takes the form of a boundary layer the maximum is near the top of this layer.

Once the puffs/plumes develop, the nonlinear inertia forces associated with the entrainment into them control their horizontal spacing which is of the order h (the most unstable wavelength of Rayleigh–Bénard convection). Since the average contribution by the surface heat flux (hF_θ) is equal to the flux carried by the bulge ($\Delta T w_* \ell$) it follows that

$$\Delta T\, w_*/F_\theta \sim h/\ell. \tag{2.4}$$

The horizontal flow into the plume/puff is of the order of w_*. Applying the advection–diffusion balance to the surface layer leads to an estimate of its thickness given by

$$\ell \sim hPe^{-1/2}. \tag{2.5}$$

These results can be expressed in terms of the Rayleigh number

$$Ra = \frac{g\beta\,(T_0 - T_h)\,h^3}{\nu\kappa}, \tag{2.6}$$

and the Nusselt and Prandtl numbers

$$Nu = \frac{F_\theta h}{\kappa\,(T_0 - T_h)}, \quad Pr = \frac{\nu}{\kappa}. \tag{2.7}$$

Since $\Delta T \sim (T_0 - T_h)$ it follows from (2.3) that

$$Ra \sim Pe^{5/2} Pr^{-1}, \tag{2.8}$$

so that with help of (2.4) we find $Nu \sim (Pr\, Ra)^{1/5}$. Other Ra–Nu relations (see Lohse & Grossmann 2000 and Castaing *et al.* 1989) result from slightly different models of eddy structure. For recent laboratory experiments up to $Ra \sim 10^{14}$ see Niemela *et al.* (2000).

The flow pattern in the instability bulge is affected to some extent by the vorticity of opposite sign generated by the no-slip condition at the base surface. This leads to an internal layer of thickness δ_v (see figure 2). For moderate values of Re and Pe, $\delta_v \sim \ell$ and this tends to produce a double maximum in the vertical velocity. Also, the vorticity generated by the friction at the surface tends to prevent the puff structure from developing into a plume.

We now consider the effect of varying the thermal diffusivity κ_b and thickness h_b of the base. Let us first introduce the length scale ℓ_b as the distance over which heat is conducted in the base on a time scale h/w_*, where

$$\ell_b \sim \sqrt{\kappa_b \frac{h}{w_*}}.$$

† In a laminar or turbulent plume from a constant-buoyancy source the peak velocity decreases with height as $w \sim (g\beta F_\theta)^{1/3} x_3^{-1/3}$. The reason why in a turbulent convective layer the *average* value of w'^2 increases slowly as $\sim x_3^{2/3}$ with height is because the plume widths increase with z and because downdraughts are blocked by the surface (Hunt 1984).

If κ_b is very large and h_b small enough so that $\kappa_b \gg \kappa$ and $\ell_b \gg h_b$, then persistent plumes tend to form, extending upwards from the surface layer towards the top of the fluid layer at $z \sim h$.

But there is a different flow pattern if the thermal diffusivity of the base is reduced. First we consider a slight reduction where $\infty > \kappa_b \gg \kappa$. We also ensure that h_b is increased sufficiently so that $\ell_b \ll h_b$. Then the heat flux from the bottom of the slab reaches the surface so 'slowly' that the surface temperature is changed significantly (by order ΔT_b within the thermal layer ℓ_b) through the downward cooling motion induced on the flanks of the puff within the time scale h/w_* during which the puff grows. ΔT_b can be estimated by equating the rate of heat gained by the fluid, as it moves along the surface, to the upward flux of heat in the base reaching the surface by conduction, i.e. $\Delta T_b w_*/h \sim F_\theta/\ell_b$. With the expression for ℓ_b given above we find that ℓ_b is less than the slab thickness h_b, if

$$Pe > \frac{\kappa_b}{\kappa}\left(\frac{h}{h_b}\right)^2. \tag{2.9}$$

Then ΔT_b is given by

$$\frac{\Delta T_b}{\Delta T} \sim \frac{\ell}{\ell_b} \sim \sqrt{\frac{\kappa}{\kappa_b}}. \tag{2.10}$$

Thus, as expected, the lower the thermal diffusivity of the slab the greater the temperature fluctuations at the surface. Note that we have assumed that the horizontal diffusion of heat in the slab (over a scale of the order h) is much smaller than the vertical diffusion, which requires that $\ell_b \ll h$.

As a result of this surface cooling, both the local density and the hydrostatic pressure rise by $O(\rho g \beta \Delta T_b \ell)$ in the surface layer. If this is of the order of the momentum of the horizontal flow into a puff, i.e. ρw_*^2, it tends to block the surface velocity feeding into the puff. Since the pressure rise is greatest at the surface and the horizontal velocity is greatest at the top of the layer, the puffs are only suppressed if $g\beta\Delta T_b \ell \gtrsim w_*^2$ or from (2.3) and (2.10)

$$\frac{\ell}{\ell_b} \gg 1 \quad \text{or} \quad \frac{\kappa_b}{\kappa} \ll 1. \tag{2.11}$$

Since $u_i \partial p/\partial x_i > 0$, this induces a change in surface velocity away from the puff, see figure 2(*a*)(i). Therefore, for $\kappa_b \ll \kappa$, over the period h/w_* when the base near the puff is cooling, the source of warm fluid into the puff is cut off. The buoyant fluid in the puff, that was produced before the surface cooled, rises from the surface as a coherent vertical eddy, similar to a vortex ring (see figure 2*b*). This suggests that plumes or larger puffs can only form if the surface is not significantly cooled by the heat flow into the puff. Also it implies that where puffs form as a result of small base diffusivity the spatial variation of the surface temperature is of the order of the scale of the puffs. This is of the order ℓ near the surface layer, and is a reduction by a factor of $O(\ell/h)$ from the scale with a high-diffusivity base. A similar reduction in time scale occurs because large puffs cannot be formed.

Even if $1 \gtrsim \kappa_b/\kappa$ so that the horizontal pressure gradient in the surface layer is not large enough to stop the formation of plumes directly, there can be a transformation of their structure caused by the time-dependent behaviour of the heat flux into the plumes that form above the surface layer. Consider what happens if the flux of buoyant fluid rising from the base of a plume decreases significantly in the time h/w_* that it takes the fluid situated initially between the levels $x_3^{(1)}$ and $x_3^{(2)}$ (see figure 2*c*, ii)

to reach the upper boundary. It is found from a simple analysis of such an unsteady plume (Morton *et al.* 1956) that the plume breaks up into elongated puffs because the more buoyant upper region entrains external fluid into the lower region where the upward buoyant motion is weaker. This causes the plume to 'pinch-off' and hence generates an elongated puff.

At much higher Reynolds numbers, the flow in the surface layer and in the interior of puffs and plumes is highly turbulent with eddies generated by local buoyancy forces. Where the surface layer meets the lower surface at $x_3 = 0$ there is a local logarithmic shear profile (Sykes, Henn & Lewellyn 1993) which is determined by small eddies blocked by the surface. The thickness of the surface layer is found to be of the order of $\ell \sim h/10$ (Hunt 1984). (Note that this is much larger than if the surface layer were laminar at the same Reynolds number.) Within this layer where the horizontal velocity profile (on the time scale of the plumes/puffs) is logarithmic (Sykes *et al.* 1993) there is a much thinner surface shear layer. Its depth $\mathscr{L}$ is determined by the equilibrium between the local rates of production of turbulent energy and dissipation (e.g. Townsend 1976) so that $\mathscr{L} = u_{*_c}^3/\varepsilon_*$. Here ε_* is the rate of dissipation in the core, i.e. $\varepsilon_* \sim w_*^3/h \sim g\beta F_{\theta 0}$, and the local surface friction velocity driven by the large eddies is $u_{*_c} \sim w_*/\ln(\ell/z_0)$ (Hunt 1998). This implies that $\mathscr{L}$ is equal to the local Monin–Obukhov length scale. In this case, the much thinner vortical layer generated by the surface friction does not significantly affect the development of plumes/puffs at the top of the surface layer (unlike the case of lower Reynolds number convection) as illustrated in figure 2(*b*).

Now, as before, let us consider the base conductance κ_b to be small while the base is deep enough that the horizontal heat flux in the base cannot even out the surface temperature changes as a result of the advection by eddies (i.e. $\ell_b \ll h_b$). The surface temperature then decreases on the horizontal scale ℓ_b towards the locations of puffs/plumes (though it rises to a local maximum just under the puff/plume where the surface velocity is zero, see figure 2*a*, i). Because the surface layer is highly turbulent and well mixed, most of the temperature decrease in the fluid (caused by the surface cooling) occurs across the thin surface shear layer of thickness is of order $\mathscr{L}$. This is much less than ℓ. The hydrostatic pressure variation can then be estimated as

$$g\beta \Delta T_b \mathscr{L} \sim \frac{g\beta F_\theta \mathscr{L} h}{w_* \ell_b}. \tag{2.12a}$$

This should be much greater than w_*^2 for plumes to be affected by the change in heat flux. With the expressions for ℓ_b and ΔT_b given above, the following criterion can then be derived for the reduced surface conductance to cause the cut-off of the plume:

$$\frac{w_* h}{\kappa_b} > \ln^6(h/z_o). \tag{2.12b}$$

Since, generally at high Reynolds number, criterion (2.12*b*) is satisfied, some other reason is needed to explain why plumes form in high-Reynolds-number atmospheric flows such as those observed by Priestley (1959). Our hypothesis is that this is because radiation processes at the ground surface provide sufficient heat input to the plumes so as to maintain a constant surface temperature. In fact on hot days and in desert climates the primary thermal balance at the surface during the day is controlled by a balance of radiation flux. Then ΔT_* in the surface layer is much less that the estimate (2.12*a*) and there is no tendency for the plume to be cut off. However, in cloudy day-time conditions, the conditions when puffs were observed by Scorer (1954), this

is not so and the heat transfer is determined more by the conduction of heat between the ground and the atmosphere.

The above analysis suggests that the surface heat conductance affects the eddy structure and the statistics in the surface layer. However, it may have much less effect on the r.m.s. and peak values of temperature in the flow, since these are largely associated with the centres of plumes and puffs (see Hunt *et al.* 1988). The average value of temperature at the surface (for a given average heat flux) depends mainly on the slow variation of temperature over the whole surface layer and therefore may not be very sensitive to the base conditions and eddy structure. These conjectures together with the other results of this analysis are now explored by the numerical simulations reported in § 3. Further geophysical examples are given in § 6.

3. Numerical simulations

3.1. *Governing equations*

The system to be simulated consists of a thermally conducting solid layer, called the base, lying below a layer of fluid. In the solid layer we need to solve only the energy equation, which reduces to a heat diffusion equation, while in the fluid layer both the momentum and energy equations need to be considered. The flow is taken to be incompressible and all fluid properties are assumed constant. To model the variation of density with temperature in the body force term, the Boussinesq approximation is used.

All variables in the equations are non-dimensionalized in terms of the depth of the fluid layer h and the convective velocity scale w_* given by (2.2). Note that the temperature scale is $\theta_* = F_\theta / w_*$, where F_θ is the correlation of the temperature and vertical velocity fluctuations at the bottom of the fluid layer. This results in the following equations for continuity, momentum and energy written in Cartesian tensor notation, for the normalized velocity components u_i, pressure p and temperature θ in the fluid layer:

$$\left.\begin{aligned} &\frac{\partial u_i}{\partial x_i} = 0, \\ &\frac{\partial u_i}{\partial t} + u_j \frac{\partial u_i}{\partial x_j} = -\frac{\partial p}{\partial x_i} + \theta \delta_{i3} + \sqrt{\frac{Pr}{Ra_*}} \frac{\partial^2 u_i}{\partial x_j^2}, \\ &\frac{\partial \theta}{\partial t} + u_j \frac{\partial \theta}{\partial x_j} = \frac{1}{\sqrt{PrRa_*}} \frac{\partial^2 \theta}{\partial x_j^2}, \end{aligned}\right\} \tag{3.1}$$

where $Pr = \nu/\kappa$ is the Prandtl number and Ra_* denotes a modified Rayleigh number based not on the temperature difference, but on the characteristic temperature θ_*. Thus

$$Ra_* = \frac{g\beta\theta_* h^3}{\nu\kappa}.$$

In the solid base the non-dimensionalised diffusion equation is

$$\frac{\partial \theta}{\partial t} = \frac{1}{\sqrt{PrRa_*}} \frac{\kappa_b}{\kappa} \frac{\partial^2 \theta}{\partial x_j^2}.$$

3.2. *Numerical details*

The velocity and temperature fields in the fluid and the temperature field in the base are solved independently as a function of time. We first assume the temperature

flux at the surface of the fluid layer to be given and use this flux at the top of the solid base as a boundary condition for the diffusion equation. The new value for the temperature flux at the upper surface of the base is then used as a boundary condition for the energy equation in the fluid layer. At the interface, the difference in diffusivity between the fluid and the solid must be taken into account. In order to represent the temperature flux at the interface $F_{\theta_i} = -k_i \partial\theta/\partial z$ correctly, we use the harmonic mean of the two conductivities given by $k_i = 2kk_b/(k + k_b)$ as the overall diffusivity at the interface (see Patankar 1980). In addition to the combined computation of the fluid layer and base we also compute convection in the fluid layer for the case of a constant flux and a constant temperature as boundary condition at the lower surface.

In the fluid, the Navier–Stokes equations and the energy equation are discretized by means of a second-order finite volume method on a staggered grid (the temperature and pressure are located in the centre of a grid cell). For the time advancement a second-order Adams–Bashforth scheme is used. In the solid, the energy equation is discretized by means of a second-order finite volume method in the vertical and a direct solver using a Fourier transform is applied in the horizontal directions. For the time advancement a backward Euler method is applied.

In the horizontal directions periodic boundary conditions are assumed for the temperature and the velocities in both the fluid layer and the base. At the lower and the upper boundary of the fluid layer a no-slip condition for the velocity is set. A zero heat flux is prescribed at the upper boundary and at the bottom of the base a heat flux $H_0 = \rho c_p F_\theta (1 + h_b/h)$ is applied so that the mean heat flux at the bottom of the fluid layer is $\rho c_p F_\theta$.

Computations are carried out for two values of the Rayleigh number, $Ra_* = 10^4$ and 10^5. In both cases the Prandtl number is $Pr = 0.7$. With $Re \equiv w_* h/\nu = \sqrt{Ra_*/Pr}$ this results in Reynolds numbers of approximately 119 and 375, respectively. Note that these Reynolds numbers are much less that the threshold value of about 10^4 above which there is a significant inertial subrange in the turbulence spectrum and the velocity profile in the surface layer is logarithmic.

The simulations are performed in a rectangular box with the aspect ratio of the fluid domain equal to 5:1. The depth of the conductive layer is the same as the depth of the fluid ($h_b = h$). The numerical mesh in the fluid layer consists of 40^3 gridpoints for $Ra_* = 10^4$ and 100^3 for $Ra_* = 10^4$. This is sufficient for fluid motions on the Kolmogorov dissipation scale η to be resolved. With the mean value of the dissipation in the fluid layer equal to $\overline{\varepsilon} = 0.5 g\beta F_\theta$ it follows that

$$\frac{\eta}{h} = \left(\frac{2Pr^{3/2}}{Ra_*^{3/2}} \right)^{1/4}, \tag{3.2}$$

so that $\eta/h \simeq 0.08$ and $\eta/h \simeq 0.014$ for $Ra_* = 10^4$ and 10^5, respectively.

The smallest temperature length scale δ_θ in the base is estimated as $\delta_\theta \sim \ell_b = \sqrt{\kappa_b h/w_*}$ which leads to

$$\frac{\delta_\theta}{h} = \sqrt{\frac{\kappa_b/\kappa}{\sqrt{Ra_* Pr}}}.$$

Thus for the mesh of 40^3 grid points and $Ra_* = 10^4$, the computation may be considered fully resolved for a ratio of $\kappa_b/\kappa > 0.05$, and for the case of 100^3 grid-points and $Ra_* = 10^5$ for $\kappa_b/\kappa > 0.01$.

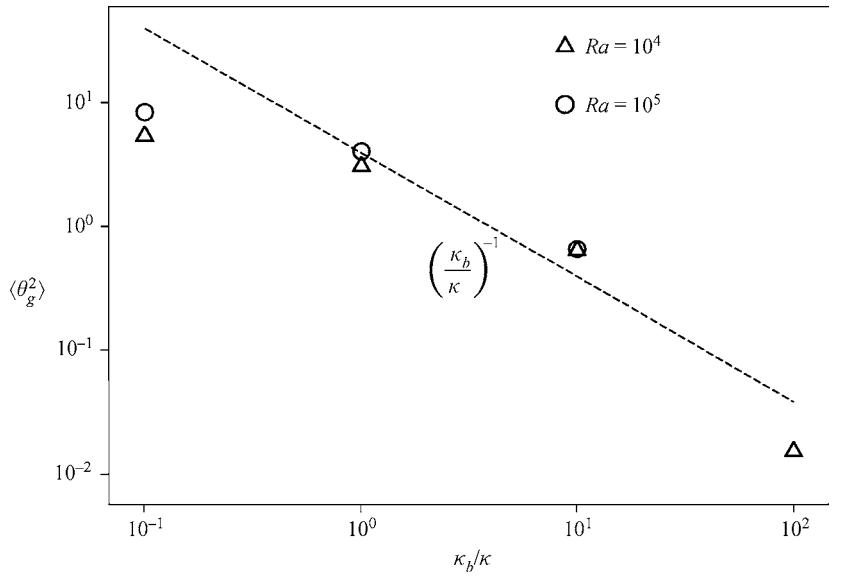

FIGURE 3. The variance of the surface temperature fluctuations normalized with θ_* as a function of the ratio κ_b/κ. The dashed line is the scaling relationship given by (2.10) which is valid only for $\kappa_b/\kappa > 1$. The angle brackets here and in subsequent figures indicate an average over a horizontal slab of the numerical simulation results.

4. Results and interpretation of the numerical simulation

In the following sections we present the results of our numerical simulations. All results pertain to a quasi-stationary boundary layer for which the total temperature flux in the fluid layer and base is a linear function of height. The statistics are computed by averaging the data over a horizontal plane and by averaging over at least 10 time scales h/w_*.

Let us first verify with help of these numerical results the scaling relationship that we have derived in §2 for the variance of the temperature fluctuations at the surface at moderate Reynolds numbers. This variance is illustrated in figure 3 for the two Ra_* cases. We find that the scaling relationship (2.10) is followed for $\kappa_b/\kappa > 1$. The deviation of the scaling relationship for $\kappa_b/\kappa < 1$ is related to the fact that the temperature rise of a fluid particle entering and leaving the surface layer cannot be greater than the mean temperature rise ΔT.

4.1. *One-point statistics*

The vertical profile of the mean value of the temperature difference non-dimensionalized by θ_*, $\theta - \theta_m$, is plotted in figure 4. Here, θ_m is computed as the vertically averaged temperature in the core, defined as ℓ, i.e. $x_3/h > 0.2$ for $Ra_* = 10^4$ and $x_3/h > 0.1$ for $Ra_* = 10^5$. The lines in figure 4 represent various values of the ratio κ_b/κ. We find that for each individual value of Ra_* the curves for different values of the ratio κ_b/κ overlap. Furthermore, when $x_3 > \ell$ the curves for the two values of Ra_* coincide. In other words, figure 4 shows convincingly that the mean temperature profiles are quite insensitive to the value of the base conductance.

There is a sharp decrease of $\theta - \theta_m$ in the fluid surface layer above the base, by a factor of 5 for $Ra_* = 10^4$ and a factor of 10 for $Ra_* = 10^5$ which is of the same order as the ratio h/ℓ as predicted by (2.4) where ℓ is the thickness of the surface layer. Note that in many measurements of the bulk properties of convection, the

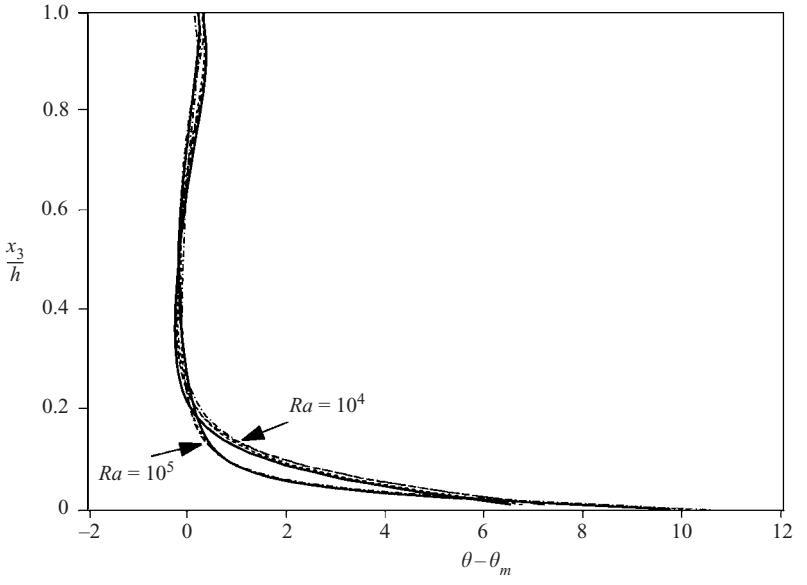

FIGURE 4. The profile of the difference of the non-dimensional mean temperature with respect to its mean value in the core of the boundary layer for two values of Ra_* The lines represent the results for values of the ratio κ_b/κ between 10 and 0.1.

temperature difference between the surface and the core is normalized on the surface flux according to

$$Nu = \frac{F_\theta h}{(T - T_m)\kappa} = \frac{Re\,Pr}{\theta - \theta_m}. \tag{4.1}$$

In the previous section we have estimated that $Re = 115$ and $Re = 375$ for the two cases that we compute here. At these low Reynolds numbers the surface layer is effectively laminar so that the linear variation of θ with x_3 in the lowest layer differs greatly from the logarithmic variation measured at very high Reynolds numbers in the surface layer of the atmospheric convective boundary layer (e.g. Kader & Yaglom 1990).

The vertical profiles of the variance of the vertical component of the velocity, $\overline{u_3^2}$, (normalized with the convective velocity w_*) are plotted in figure 5. Again we observe little sensitivity near the surface as a function of κ_b. Above the surface layer, in the middle of the fluid layer, there is some variation although there seems to be no clear dependence of this variation on the ratio κ_b/κ.

By contrast the profiles of the temperature variance $\overline{\theta'^2}$ illustrated in figure 6 show in the surface layer a clear dependence on the base conductance. Because the mean temperature gradient is greatest in the surface layer, the effect of any change in the vertical velocity fluctuations must cause the greatest difference in the peak values in this region. Note that $(\overline{\theta'^2})^{1/2}$ is a sizeable fraction of the mean temperature drop across the surface layer (about 30%) because, as the plumes/puffs grow and decay, they are continually changing the local temperature field. This is why $\overline{\theta'^2}$ is particularly sensitive to κ_b in this part of the flow. Figure 6 also shows the temperature fluctuations for the two special cases of a constant surface flux, F_θ, and a constant surface temperature. For the case of a constant flux, this leads to a much higher surface temperature in the stagnant region below the plume than for the case of a conducting base. As a result the overall level of temperature fluctuations is increased.

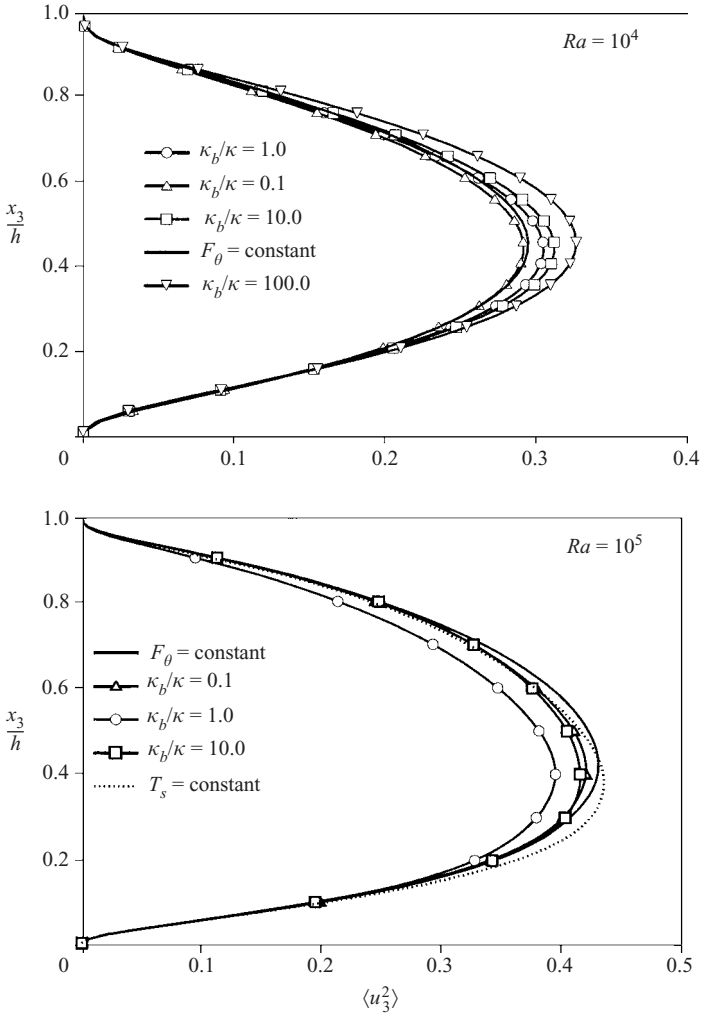

FIGURE 5. The profile of the variance of the vertical velocity fluctuations for the two cases of Ra_* non-dimensionalised with w_* for some values of the ratio κ_b/κ.

The temperature fluctuations near the surface for the case of the constant surface temperature remain quite small over the whole surface layer. It seems that the constant surface flux and the constant surface temperature are limiting cases for the ratio κ_b/κ approaching infinity and zero, respectively.

Finally, we mention that the profiles presented in this section agree well with the experimental data of Adrian, Ferreira & Boberg (1986) and the direct numerical simulations of Coleman, Ferziger & Spalart (1994).

4.2. *Real time statistics and flow visualizations*

Further insight into how the eddy motion and temperature field change, as κ_b varies, comes from examining individual realizations of these fields. Figures 7(*a*) and 7(*b*) show instantaneous contours of the temperature in the horizontal plane at the fluid–solid interface ($x_3 = 0$) for two cases of the ratio κ/κ_b. The effect of base diffusivity on the scale of the temperature variations at this interface is quite clear. In figures 7(*c*) and 7(*d*) the instantaneous temperature field at the top of the surface layer, i.e.

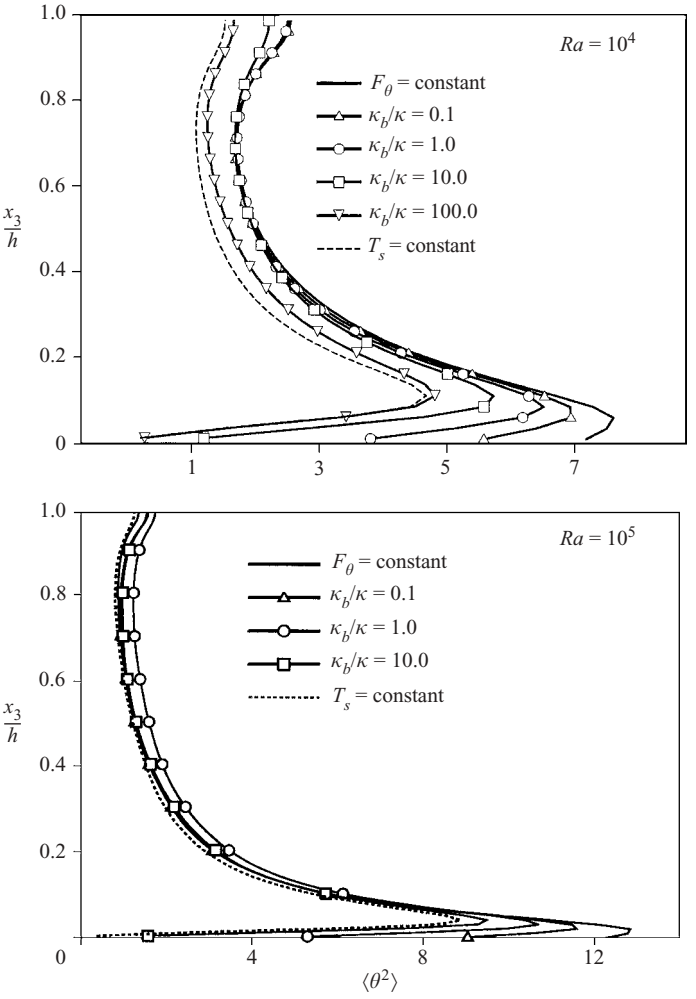

FIGURE 6. Profiles of the variance of the temperature fluctuations for the two cases of Ra_* non-dimensionalised with θ_* for some values of the ratio κ_b/κ.

$x_3 = 0.1h \sim \ell$, is illustrated. In both cases of κ/κ_b we can distinguish hexagonal patterns of bands of hot fluid, which have also been found by Schmidt & Schumann (1989) who incidentally applied a constant-flux boundary condition.

Figures 8(a) and 8(b) show contours in the vertical plane of the temperature field. It is clear that the effect of lowering the base conductance is to reduce the horizontal length scale of the temperature fluctuations close to $x_3 = 0$. But there is not much effect in the core. Note that the typical width of the puffs/plumes is about $0.25h \pm 0.05h$ thus confirming the hypothesis and many previous observations and simulations that these regions are quite thin compared to the downdraughts between them. Comparing figures 8(a) and 8(b) shows that with low base diffusivity the average vertical extent of the heated plumes is less than with higher diffusivity, where in most cases the plumes extend from the ground to the top of the fluid layer. In the former case the unsteady plumes break up into puffs and some of them reach the top. In the latter case there is a relatively steady structure that persists well beyond the time it takes for particles to travel from the surface to the top of the layer (i.e. h/w_*).

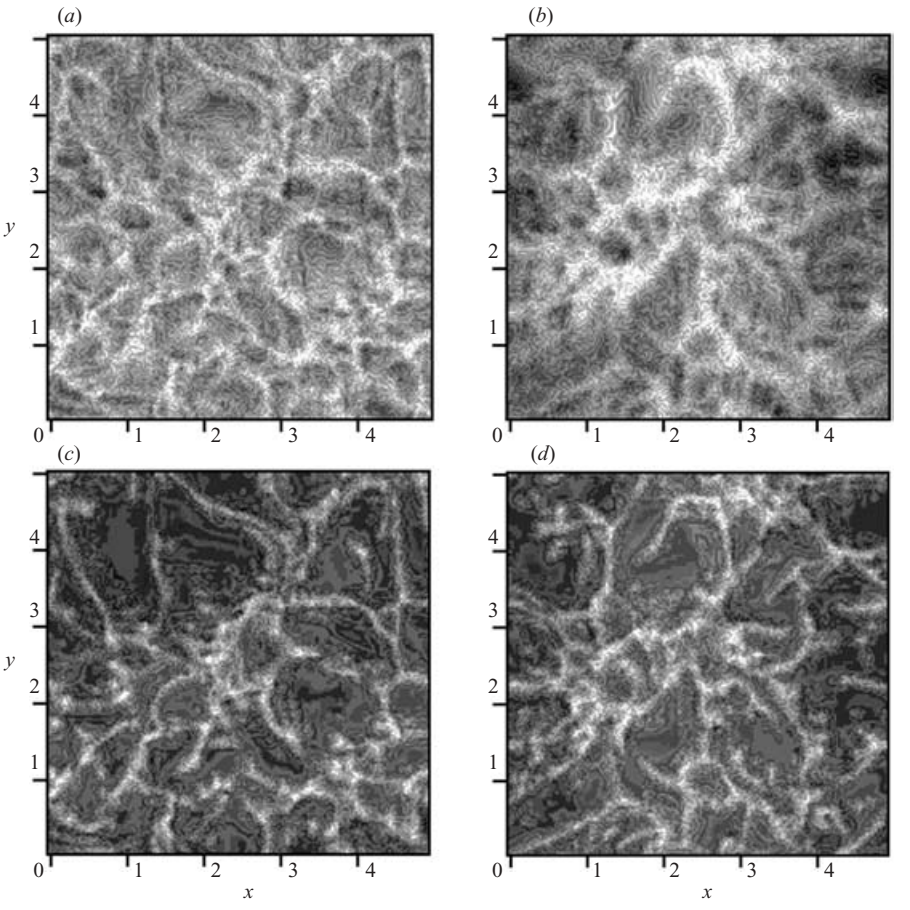

FIGURE 7. Instantaneous temperature field in the (x, y)-plane (light: hot, dark: cold) for the case $Ra_* = 10^5$ in a horizontal plane for the cases: (*a*) $\kappa_b/\kappa = 0.1$ and $x_3 = 0$; (*b*) $\kappa_b/\kappa = 10.$ and $x_3 = 0$; (*c*) $\kappa_b/\kappa = 0.1$ and $x_3 = 0.1h$; (*d*) $\kappa_b/\kappa = 10.$ and $x_3 = 0.1h$.

The effect of varying the base conductance on how plumes and puffs develop in time can be understood by the analysis of time series. Such time series have been collected at a number of x_1, x_2-positions for the following variables: the normalized surface temperature, the normalized temperature in the base at some distance below the surface and both the temperature and vertical velocity w at the top of the surface layer $x_3 = \ell$. The temperatures are corrected for the steady rise in mean temperature by subtracting a linear trend as a function of the time. As a result the average over the time series of all corrected temperatures is zero. The corrected temperatures are indicated by θ'_g, $\theta'_{x_3=-0.1h}$ and $\theta'_{x_3=0.1h}$ for the surface temperature, the temperature in the base and the temperature in the fluid layer, respectively. Based on the time series of the surface temperature we define events as occurrences where θ'_g deviates by more than one standard deviation from its mean and these are denoted as a 'hot surface event'. We show in figure 9 an average 'hot surface event' by taking the mean over four individual events where the time origin has been centred on each event. Note that all temperatures have been scaled with the value of θ'_g at time $t = 0$. The results of a similar analysis where θ'_g is less than one standard deviation below the mean values is shown in figure 10 as a 'cool surface event'.

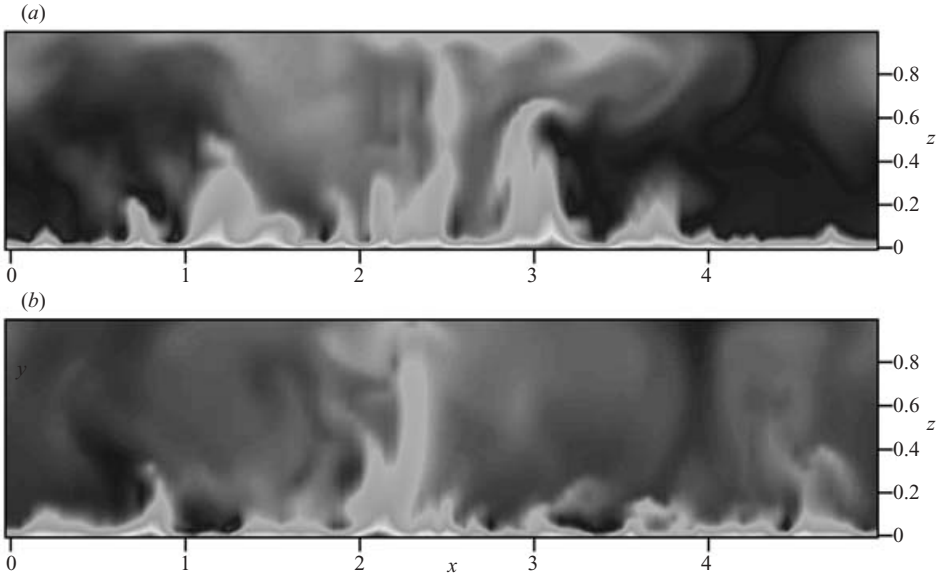

FIGURE 8. Instantaneous temperature field in the (x, z)-plane (light: hot, dark: cold) for the case $Ra_* = 10^5$ in a vertical plane for the cases: (*a*) $\kappa_b/\kappa = 10$; (*b*) $\kappa_b/\kappa = 0.1$.

Both figures 9 and 10 suggest that the time scale of an event is smaller than h/w_* irrespective of the ratio κ_b/κ. As the horizontal velocity of a plume/puff is estimated to be $0.1w_*$ and its width about $0.25h$, a typical plume/puff moves at most a distance of about 1/4 of its width during its evolution time as indicated in figure 2. The figures 9 and 10 also suggest that the plume/puff strength varies with time over a period of about $0.5h/w_*$. Furthermore, it follows from figure 9 that when θ_g' reaches its maximum, the temperature and vertical velocity at $x_3 = 0.1h$ reach their maximum somewhat earlier. The temperature and vertical velocity at $x_3 = 0.1h$ appear to be well correlated. Note how the cooling events shown in figure 10 are also associated with lateral movements, which explains the asymmetry of the curves. For the cases with $\kappa_b/\kappa = 0.1$, regions where the surface cools, i.e. $\partial T_g/\partial t < 0$, coincide with regions where $u_3 < 0$, corresponding to core fluid impinging on the surface.

Both figures 9(*a*) and 9(*b*) show that the fluid near the base has its maximum temperature in the local stagnation flow just after the plume centreline passes this point. Here the vertical velocity reaches its maximum velocity of about $0.7w_*$. The reason for this delay is that both plumes and puffs move, which produces a warm wake on the 'trailing' side of these eddies (as it does with jets placed perpendicular to a cross-flow, Coelho & Hunt 1989). Note that the plume ($\kappa_b/\kappa = 10$) has a deeper wake, while in the puff case ($\kappa_b/\kappa = 0.1$) the surface temperature recovers more quickly (see figure 9*c*). This is because outside the rising puff there are downdraughts of slowly moving cooler fluid. This fluid is entrained into the base region of the puff quite close to the puff centreline (see figure 2*c*).

4.3. *Time and space cross-correlation*

The previous discussion on the changes in space and time structure of puffs/plumes as the base diffusivity varies can be tested by examining the changes in the time and space cross-correlations of u_3 and θ.

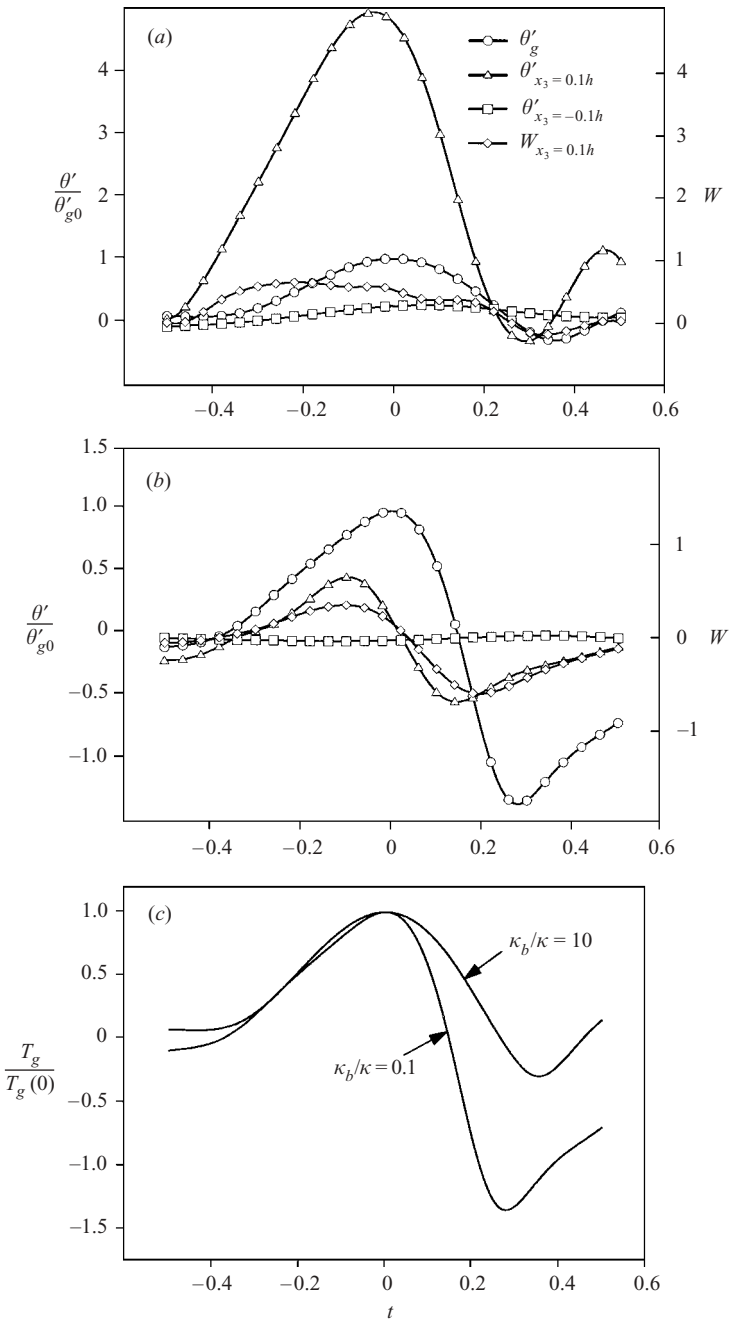

FIGURE 9. Hot surface events; the time evolution of the temperature fluctuation at three heights and the vertical velocity at one height for an event where the fluctuating surface temperature $\theta'_g = \theta'(x_3 = 0)$ is larger than the mean plus one standard deviation. The results shown denote the average over four individual events. The time when θ'_g reaches its maximum has been taken as the origin. All temperatures shown have been scaled with the value of θ'_g at the time equal to zero, θ_{g0}. (*a*) $\kappa_b/\kappa = 10$; (*b*) $\kappa_b/\kappa = 0.1$; (*c*) comparison of the time variation of θ'_g/θ_{g0} between the high and the low base thermal diffusivities.

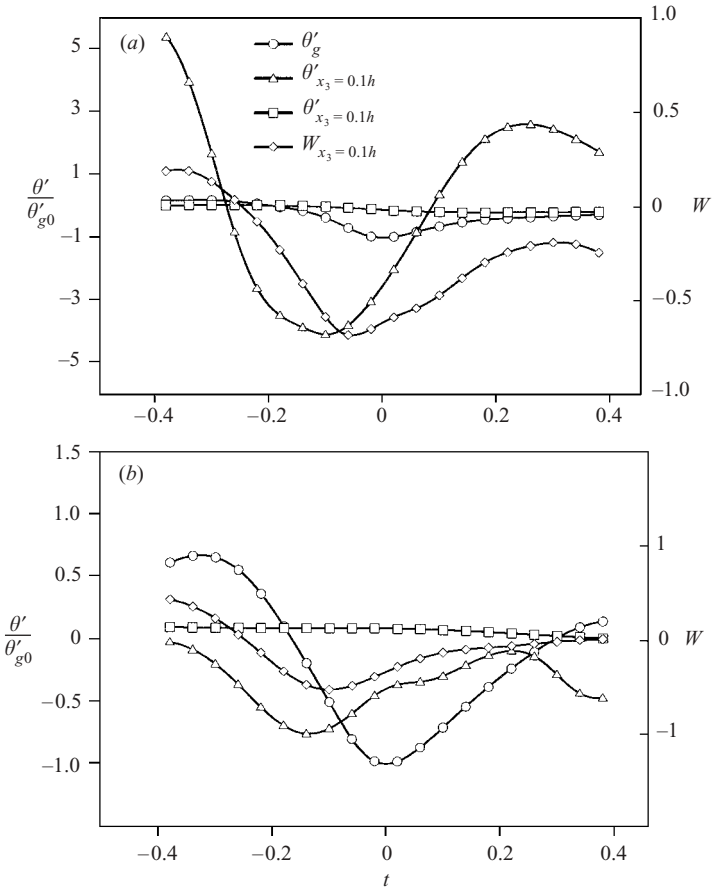

FIGURE 10. Cool surface events; the time evolution of the temperature fluctuation at three heights and the vertical velocity at one height for an event where the fluctuating surface temperature $\theta'_g = \theta'(x_3 = 0)$ is smaller than the mean minus one standard deviation. The results shown denote the average over four individual events. The time when θ'_g reaches its maximum has been taken as the origin. All temperatures shown have been scaled with the value of θ'_g at the time equal to zero, θ_{g0}. (*a*) $\kappa_b/\kappa = 10$ and (*b*) $\kappa_b/\kappa = 0.1$.

First, figure 11(*b*) shows that at the top of the surface layer the integral scale of the temperature fluctuation is not affected by the reduction of the base diffusivity. This is consistent with qualitative examination of figure 7, which shows that the transition of plumes to elongated puffs as κ_b decreases does not affect their horizontal scale. By contrast figures 11(*a*) and 11(*b*) confirm the qualitative picture shown in figure 7 that at the surface ($x_3 = 0$), when the base diffusivity is low, there is a significant reduction by 40% of the horizontal temperature length scales.

The autocorrelation for the temperature fluctuations and velocity fluctuations at the surface and at the top of the surface layer is plotted in figures 12(*a*) and 12(*b*). It shows that the time scale of the eddy motion is reduced by about 30% by the reduction of the thermal diffusivity of the base. Unlike the spatial structure, which is only reduced at the surface, the time scales are also reduced in the interior of the convective region. This is consistent with our concept discussed in § 2. The reduction of κ_b to a value less than κ leads to shortened plumes or elongated puffs with a

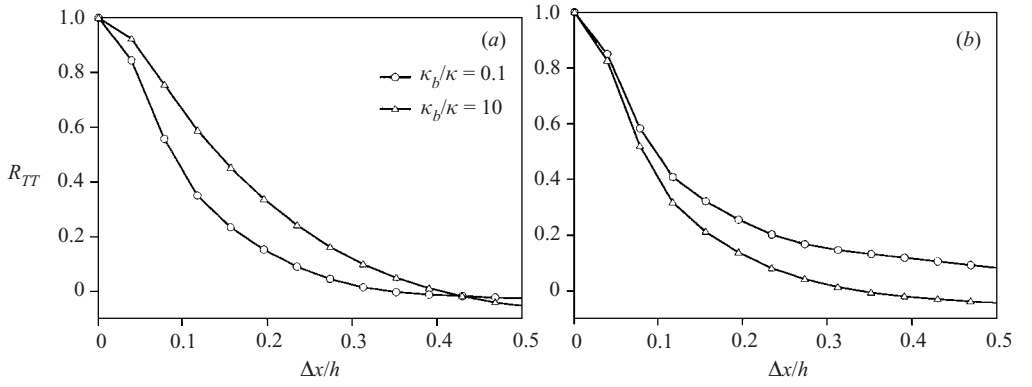

FIGURE 11. Spatial correlation of the temperature fluctuations for the two cases of κ_b/κ: (*a*) at the fluid–base interface $x_3 = 0$; (*b*) at the top of the surface layer $x_3 = 0.1$;

similar spatial form in the lower part of the convective layer as for high κ_b. They also have a shorter time scale as they re-form slightly more frequently than the steadier plumes which extend right to the top of the fluid layer when $\kappa_b \gg 1$.

5. Qualitative laboratory experiments

To explore the general concepts developed here a qualitative laboratory test was conducted in the Environmental Fluid Dynamics Laboratory at Arizona State University.

A square ($0.3 \times 0.3\,\mathrm{m}^2$) glass tank with an aluminium base with a thickness of $h_b = 1$ mm was heated by contact with an electrically heated ceramic plate. The depth h of water within the tank was 0.1 m and $\kappa = 10^{-6}\,\mathrm{m}^2\,\mathrm{s}^{-1}$. The flow was visualized with neutrally buoyant particles of about 2 mm in diameter. The experimental flow patterns were recorded by video. The typical velocity in the tank was $0.01\,\mathrm{m\,s}^{-1}$ so that the value of the Reynolds number becomes $Re \simeq 10^3$. With $\kappa_b = 10^{-4}\,\mathrm{m}^2\,\mathrm{s}^{-1}$ the characteristic thermal distance $\ell_b = (\kappa_b h/w_*)^{1/2} \simeq 30$ mm. Thus $\ell_b \gg h_b$, so that the base provided an effectively constant heat flux. In this situation the criteria for unsteady plume behaviour (see equations (2.9)–(2.11)) are not exceeded and therefore steady conditions can be expected. In fact a steady plume was observed, as in other experiments for similar conditions. In this case the plume centreline was located at about a third the distance along the tank. The horizontal flow at the bottom boundary moved steadily into the plume.

In the second experiment a 15 mm aluminium plate was attached at the bottom of the tank with a tight fit so that there was good thermal contact. Immediately the flow structure changed. The plume, while remaining vertical, moved continuously and bodily around the tank, and smaller puffs were observed growing from the bottom. In this case ℓ_b is still greater than h_b but the unsteady behaviour was quite noticeable especially at the surface.

Finally a small air gap of about 1 mm was introduced between the tank bottom and the thick plate. This reduced the effective value of κ_b for the solid base by a factor of about 4 and thence ℓ_b to a value less than h_b. A further substantial change in eddy motion occurred near the lower surface, which became quite unsteady and took the form of random puffs, with a length scale of about 1/5 of the depth of the convecting layer (h). This was a significantly smaller scale than of the plume in the

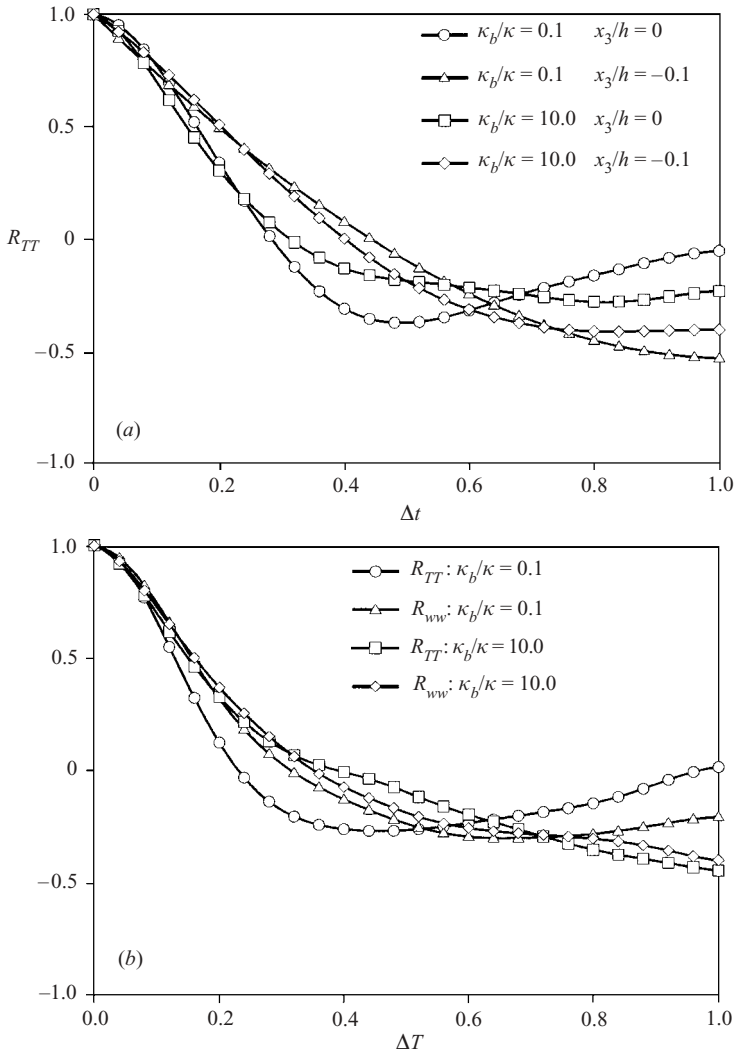

FIGURE 12. (*a*) Time correlation of the temperature fluctuations for the two cases of κ_b/κ at and below the fluid solid interface. (*b*) Time correlation of the temperature and vertical velocity fluctuations for the two cases of κ_b/κ at $x_3/h = 0.1$.

previous cases. Occasional unsteady elongated puffs were observed above the surface layer, which varied in length up to about $h/2$. Note that in this flow at values of the Reynolds number higher than the DNS, transition to puffs occurs even when $\kappa_b \simeq 10\kappa$.

These results are consistent with the concepts derived in § 2 and our numerical simulations.

6. Discussion and conclusions

A number of connected concepts about convection over solid surfaces with finite conductivities arise from our order-of-magnitude analysis, numerical simulation and visualisation experiment and from other studies. First, if the surface temperature

or surface heat flux is effectively constant, then the unstable stratification of the fluid near the surface generates persistent plumes that extent upward through the convective layer. For solid bases heated from below and which have a finite thickness h_b this situation only occurs in a certain parameter range. Plumes can also form with other heat transfer processes at the solid–fluid interface such as large radiation fluxes. These keep the surface temperature constant independently of the base diffusivity. If the Reynolds number is not so large that the surface layer is not highly turbulent (i.e. $w_* h/\nu < 10^3$), then for a 'thick' base in which the heat transfer varies on a time scale that is large compared to the eddy time, i.e. $w_* h_b/\kappa_b \gg 1$, plumes occurs only if the base thermal diffusivity is high relative to that of the fluid $\kappa_b/\kappa > 1$.

However, if the Reynolds number is very large, i.e. $w_* h/\nu > 10^4$, and when molecular diffusion processes are negligible in the flow, for a typical rough surface we conclude that plumes cannot occur – unless there is a special heat transfer process which ensures that the surface temperature is effectively uniform and largely unaffected by the heat transferred through the eddy motion. In the atmospheric boundary layer this occurs when the heat transfer at the surface is dominated by the radiation.

Secondly this study shows that if the base is thick (i.e. $w_* h_b/\kappa_b > 1$), if the Reynolds number is moderate (i.e. $w_* h/\nu < 10^3$) and if the base thermal diffusivity is less than that of the fluid (i.e $\kappa_b/\kappa < 1$) the primary eddy motion has reduced vertical and horizontal length scales (especially near the bottom surface) and a smaller time scale. When $\kappa_b/\kappa < 1$ these unsteady eddies have the form of finite-length plumes emerging from the surface layer which break off into elongated puffs.

When $\kappa_b/\kappa \ll 1$ the vertical scales of the puffs decrease and spherical-like puffs form in the surface layer. But they grow in scale as they rise through the convective layer. A notable feature of this distinction in the form of eddy motion is that it greatly affects neither the overall heat transfer rate (i.e. Nu) nor the r.m.s. value of the velocity fluctuations in the central part of the fluid layer.

These concepts can be applied even when convection is driven by other kinds of buoyancy fluxes or when affected by other kinds of flow processes. For example when thermal convection is combined with mean shear, the formation of buoyant eddies is strengthened by the enhanced mixing in the surface layer as if the base had a higher thermal diffusivity (Hunt 1998). As the shear stress increases in these flows, plumes form which are aligned with the mean velocity and are reinforced by the natural vortices formed in shear layers that are aligned with the mean flow (Townsend 1976). When there is 'compositional' convection driven by the release of higher (or heavier) fluid from the layer near the boundary, the eddy motion depends on how the buoyancy fluxes vary with the fluctuation in the compositional concentration affected by the eddies (by analogy with the temperature fields considered here). Since in geophysical convection, such as in the Earth's core or below freezing sea ice, the Reynolds number is very large ($Re \gg 10^4$), the mechanism for the formation of puffs dominates because effectively the compositional layer is not very highly diffusive (even if it is turbulent) relative to the time scale of the convective eddies. This explanation is consistent with the numerical simulation of Höllerbach & Jones (1993) and Backhaus & Kämpf (1999) which show puff- rather than plume-like eddy structure. The latter predictions have been confirmed by the recent acoustic measurements of velocity fluctuations in turbulent convection in the Arctic ocean by Uscinski *et al.* (2003). In particular they found that the typical velocity of the puffs was about equal to w_* (see § 2).

The reduction in the time scales of the eddy structure from those of plumes to puffs is significant for these two geophysical process. In the first case it amplifies the generation of the unsteady electrical currents that sustain the Earth's geo-dynamo

and causes the fluctuation and even reversal of the magnetic field. In the second case it enhances the generation of internal waves in the stably stratified layer below the convective layer and thereby thickens the layer (e.g. Fernando & Hunt 1997). Although w_* increases in proportion to $h^{1/3}$, the frequency of the characteristic waves w_*/h decreases and therefore a new equilibrium structure of the convective layer is established.

In these and other types of convection, the boundary of the convective zone may be a fluid boundary across which the convective eddy motion is coupled to eddy motion in another layer. An example is the case where convection in the atmosphere is driven by a warm ocean, especially in the high latitudes where radiation is less significant. Typically, within the ocean's 'mixed' layer below the surface, there are turbulent motions with a r.m.s. velocity u_b and a length scale ℓ_b. Because of the air/water density difference, the ocean acts as like a solid base but with a thermal diffusivity that is much larger than that of a solid because it is equal to the eddy diffusivity in the mixed layer. The vertical eddy diffusivity is

$$K_b \sim u_b \ell_b.$$

But the effect of the ocean mixed layer on the atmospheric convective turbulence depends on whether it can transport heat horizontally over the scale of the fluctuations in the atmospheric temperature. These occur over a length scale that is much larger than ℓ_b, being determined by the scale (h) of the large convective eddies in the atmosphere (where typically $h \sim 10^3$ m). This transport is determined by the longitudinal diffusivity K_b', which, as explained by G. I. Taylor (Taylor 1954), is larger than κ_b as a result of the shear motion in the mixed layer. From Sullivan's (1971) experiments and numerical study of this effect $K_b' \sim 10 u_b \ell_b$. Therefore, the ratio criterion for the formation of plumes in high-Reynolds-number convective turbulence is satisfied if

$$\frac{K_b'}{w_* h} \sim \frac{10 u_b \ell_b}{w_* h} > \frac{1}{\ln (h/z_0)}.$$

For typical magnitudes ($u_b \sim 0.01$–$0.1\,\mathrm{m\,s^{-1}}$, $\ell_b \sim 10$–100 m, $w_* \sim 1\,\mathrm{m\,s^{-1}}$, $h \sim 10^3$ m and $z_0 \sim 10^{-2}$ m) these two quantities are of the same order of magnitude and therefore plumes or elongated puffs can exist in the atmosphere above the ocean surface as is frequently found in satellite photographs (e.g. Houghton 1991).

We are grateful for enlightening conversations with A. A. Grachev, S. Zilitinkevich, C. A. Jones, M. R. E. Proctor and B. J. Uscinski. J. C. R. H. & H. J. S. F. acknowledge support from the National Science Foundation and J. C. R. H. from the Natural Environmental Research Council and the Center for Polar Observation and Modelling at UCL.

REFERENCES

Adrian, R. J., Ferreira, R. T. D. S. & Boberg, T. 1986 Turbulent thermal convection in wide horizontal fluid layers. *Exps. Fluids* **4**, 121–141.

Backhaus, J. O. & Kämpf, J. 1999 Simulations of sub-mesoscale oceanic convection and ice-ocean interactions in the Greenland sea. *Deep-Sea Res.* **46**, 1427–1455.

Castaing, B., Gunaratne, G., Heslot, F., Kadanoff, L., Libchaber, A., Thomae, S., Wu, X. Z., Zaleski, S. & Zanetti, G. 1989 Scaling of hard thermal turbulence in Rayleigh–Bénard convection. *J. Fluid Mech.* **204**, 1–30.

Coelho, S. L. V. & Hunt, J. C. R. 1989 The dynamics of the near field of strong jet in crossflows. *J. Fluid Mech.* **200**, 95–120.

Coleman, G. N., Ferziger, J. H. & Spalart, P. R. 1994 A numerical study of the convective boundary layer. *Boundary-Layer Met.* **70**, 247–272.

Deardorff, J. W., Willis, G. E. & Lilly, D. K. 1967 Laboratory investigation of non-steady penetrative convection. *J. Fluid Mech.* **35**, 7–31.

Fernando, H. J. S. & Hunt, J. C. R. 1997 Turbulence, waves and mixing at shear-free density interfaces. Part 1. A theoretical model. *J. Fluid Mech.* **347**, 197–234.

Hollerback, R. & Jones, C. A. 1993 Influence of the earth's inner core on geomagnetic fluctuations and reversals. *Nature* **367**, 541.

Holmes, P., Lumley, J. L. & Berkooz, G. 1996 *Turbulence, Coherent Structures, Dynamical Systems and Symmetry*. Cambridge University Press.

Holtslag, A. A. M. & Nieuwstadt, F. T. M. 1986 Scaling the atmospheric boundary layer. *Boundary-Layer Met.* **36**, 201–209.

Houghton, J. T. 1991 *The Physics of Atmospheres*. Cambridge University Press.

Hunt, J. C. R. 1984 Turbulence structure in thermal convection and shear-free boundary layers *J. Fluid Mech.* **138**, 161–184.

Hunt, J. C. R. 1998 Eddy dynamics and kinematics of convective turbulence. In *Buoyant Convection in Geophysical Flows* (ed. E. J. Plate, E. Fedorovich, D. X. Viegas & J. C. Wyngaard). Kluwer.

Hunt, J. C. R., Kaimal, J. C. & Gaynor, J. E. 1988 Eddy structure in the convective boundary layer – new measurements and new concepts *Q. J. R. Met. Soc.* **114**, 827–858.

Kader, B. A. & Yaglom, A. M. 1990 Mean fields and fluctuation moments in unstably stratified turbulent boundary layers. *J. Fluid Mech.* **212**, 637–662.

Kaimal, J. C., Wyngaard, J. C., Haugen, D. A., Cote, O. R., Izumi, Y., Caughey, S. J. & Readings, C. J. 1976 Turbulence structure in the convective boundary layer. *J. Atmos. Sci.* **33**, 2152–2169.

Lohse, D. & Grossmann, S. 2000 Scaling in thermal convection: a unifying theory. *J. Fluid Mech.* **407**, 27–56.

Morton, B. T. Taylor, G. I. & Turner, J. S. 1956 Turbulent gravitational convection from maintained and istantaneous source. *Proc. R. Soc. Lond.* A **407**, 1–23.

Niemela, J. J., Skreb, L., Sreenivasan, K. R. & Donelly, R. J. 2000 Turbulent convection at very high Rayleigh numbers. *Nature* **404**, 837–840.

Patankar, S. V. 1980 *Numerical Heat Transfer and Fluid Flow*. Hemisphere.

Priestley, C. H. B. 1959 *Turbulent Transfer in the Lower Atmosphere*. University of Chicago Press.

Schmidt, H. & Schumann, U. 1989 Coherent structure of the convective boundary layer derived from large eddy simulation. *J. Fluid Mech.* **200**, 511–562.

Scorer, R. S. 1954 The nature of convection as revealed by soaring birds and dragonflies. *Q. J. R. Met. Soc.* **80**, 68–77.

Scorer, R. S. 1978 *Environmental Aerodynamics*. Ellis Horwoord.

Sullivan, P. J. 1971 Longitudinal dispersion within a two-dimensional turbulent shear flow. *J. Fluid Mech.* **49**, 557–576.

Sykes, R. I., Henn, D. I. & Lewellen, W. S. 1993 Surface layer description under free-convection conditions. *Q. J. R. Met. Soc.* **119**, 409–421.

Taylor, G. I. 1954 The dispersion of matter in turbulent flow through a pipe. *Proc. R. Soc. Lond.* A **223**, 446–468.

Townsend, A. A. 1959 Temperature fluctuations over a heated horizontal surface. *J. Fluid Mech.* **5**, 209–241.

Townsend, A. A. 1976 *Structure of Turbulent Shear Flow*. Cambridge University Press.

Uscinski, B. J., Kaletsky, A., Stanek, C. J. & Rouseff, D. 2003 An acoustic shadowgraph trail to detect convection in the arctic. *Waves in Random Media* (to appear).